Drug Resistance

International Edition: DOI: 10.1002/anie.201504329
German Edition: DOI: 10.1002/ange.201504329

# Intracellular Self-Assembly of Taxol Nanoparticles for Overcoming Multidrug Resistance**

*Yue Yuan, Lin Wang, Wei Du, Zhanling Ding, Jia Zhang, Tao Han, Linna An, Huafeng Zhang,* and Gaolin Liang**

***Abstract:*** *Multidrug resistance (MDR) remains the biggest challenge in treating cancers. Herein we propose the intracellular self-assembly of nanodrugs as a new strategy for overcoming MDR. By employing a biocompatible condensation reaction, we rationally designed a taxol derivative Ac-Arg-Val-Arg-Arg-Cys(StBu)-Lys(taxol)-2-cyanobenzothiazole (CBT-Taxol) which could be subjected to furin-controlled condensation and self-assembly of taxol nanoparticles (Taxol-NPs). In vitro and in vivo studies indicated that, compared with taxol, CBT-Taxol showed a 4.5-fold or 1.5-fold increase in anti-MDR effects, respectively, on taxol-resistant HCT 116 cancer cells or tumors without being toxic to the cells or the mice. Our results demonstrate that structuring protease-susceptible agents and assembling them intracellularly into nanodrugs could be a new optimal strategy for overcoming MDR.*

Multidrug resistance (MDR) is one of the primary contributors to the failure of many chemotherapeutic agents for cancer.[1] MDR generally arises from increased expression of cellular membrane proteins that mediate unidirectional energy-dependent drug efflux, thereby causing interception and exportation of the drug before it reaches its intracellular target.[2] Normally, MDR results from the original resistance induced by one drug.[3]

[*] Y. Yuan,[+] W. Du, Z. Ding, J. Zhang, T. Han, L. An, Prof. G. Liang
CAS Key Laboratory of Soft Matter Chemistry
Department of Chemistry
University of Science and Technology of China
96 Jinzhai Road, Hefei, Anhui 230026 (China)
E-mail: gliang@ustc.edu.cn
Homepage: http://lianglab.ustc.edu.cn
L. Wang,[+] Prof. H. Zhang
School of Life Sciences
University of Science and Technology of China
Hefei, Anhui 230027 (China)
E-mail: hzhang22@ustc.edu.cn
[+] These authors contributed equally to this work.

[**] We are grateful to Shuoguo Li (Center for Biological Imaging, Institute of Biophysics Chinese Academy of Sciences), for her assistance in 3D-SIM imaging. This work was supported by the Collaborative Innovation Center of Suzhou Nano Science and Technology, the Major program of the Development Foundation of the Hefei Center for Physical Science and Technology, the National Natural Science Foundation of China (Grants 21175122, 21375121, 31171358, and 31371429), National Basic Key Research Program of China (2014CB910604), and Anhui Provincial Natural Science Foundation (Grant 1508085JGD06).

Supporting information for this article is available on the WWW under http://dx.doi.org/10.1002/anie.201504329.

The three common strategies proposed and investigated to overcome MDR are: 1) Inhibiting MDR efflux pumps with P-glycoprotein (Pgp) specific peptides or antibodies, or down-regulating the MDR1 gene with transcriptional repressors or siRNAs;[4–10] 2) structuring new agents that are less susceptible to MDR;[11,12] 3) increasing the circulation time of drugs in cells by nanocarries including liposomes, polymer conjugates, micelles, dendrimers, and carbon-based as well as metallic nanoparticles.[13,14] However, the efficacy of anti-MDR approaches through inhibitors, repressors, or siRNAs has been compromised by bioavailability problems, adverse interactions with drug performance, or interference with drug clearance, which results in elevated drug concentrations in plasma and associated toxicity.[15,16] Therefore, modification of the drug itself seems to be a better alternative strategy for overcoming MDR.[17,18] Studies have shown that certain agents (e.g. molecular transporters containing cell-penetrating peptides), when attached to a drug or probe, will facilitate their cellular uptake through multiple mechanisms other than passive diffusion.[15,19] However, cells can adapt to and resist the new agents after one circle of treatment. As a consequence of their ability to load large amount of drugs, nanocarriers have shown unique advantages for overcoming MDR by local release of a high concentration of drugs inside cells after they translocate the cell membrane. However, the difficulties of their cell translocation and fabrication, poor reproducibility or physical stability, and long-term toxicity as well as the low bioavailability of the nanodrugs eclipse their advantages in anti-MDR approaches.[20]

After considering the above-mentioned advantages and disadvantages of pre-existing anti-MDR methods, we proposed a new strategy for overcoming the MDR of drug-resistant cells in vitro and in vivo (Figure 1). Based on a biocompatible condensation reaction recently developed by Rao, Liang, and co-workers,[21–24] we designed our taxol derivative CBT-Taxol with the following components: a 2-cyanobenzothiazole (CBT) motif, a taxol motif conjugating to the side chain of a lysine (Lys) motif, a disulfide-functionalized cysteine (Cys) motif, and a RVRR substrate for furin cleavage and improving the cellular uptake of the drug.[25] The trans-Golgi protease furin is one type of protein convertases that plays important roles in homeostasis and in diseases ranging from Alzheimer to anthrax, Ebola fever, and cancer.[26] After CBT-Taxol enters into furin-overexpressed cells (i.e. HCT 116 cells here), it undergoes reduction with glutathione (GSH) and a condensation reaction controlled by furin cleavage to yield hydrophobic oligomers (mostly dimers), as demonstrated previously.[21–23] The oligomers will then self-assemble into taxol nanoparticles (Taxol-NPs) at (or

  

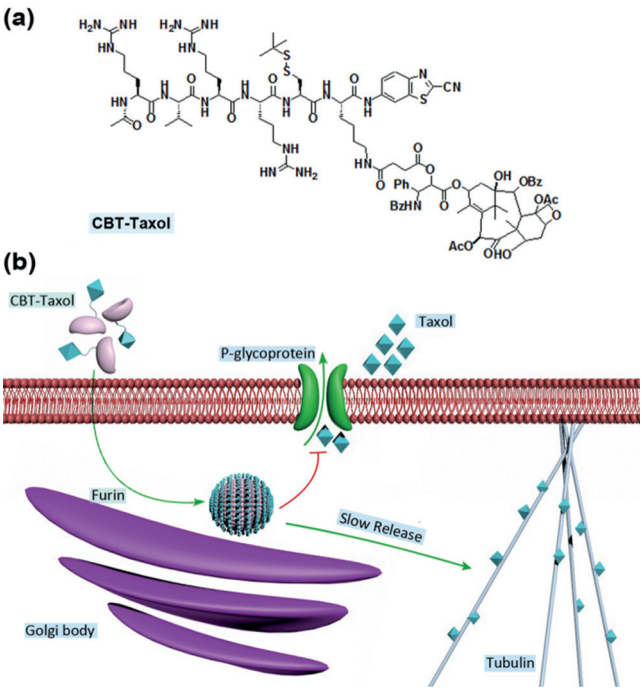


***Figure 1.*** a) Chemical structures of CBT-Taxol. b) Schematic illustration of intracellular furin-controlled self-assembly of Taxol-NPs for anti-MDR.

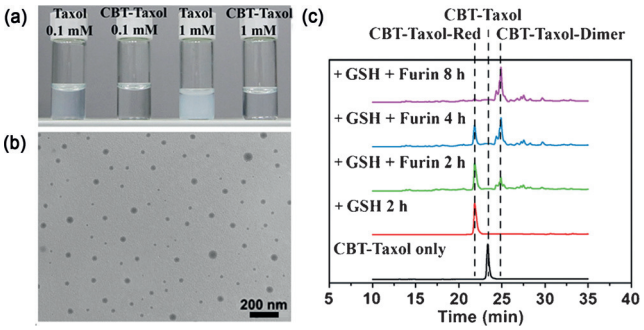


***Figure 2.*** a) From left to right: 0.1 mM taxol in water (1% DMSO), 0.1 mM CBT-Taxol in water (1% DMSO), 1 mM taxol in water (10% DMSO), 1 mM CBT-Taxol in water (10% DMSO). b) TEM images of Taxol-NPs formed by 100 μM CBT-Taxol treated with 0.2 nmol $U^{-1}$ furin at 37 °C for 8 h. c) HPLC traces of 100 μM CBT-Taxol (black), 100 μM CBT-Taxol treated with 1 mM GSH for 2 h (red), 100 μM CBT-Taxol treated with 1 mM GSH and 0.2 nmol $U^{-1}$ furin at 37 °C for 2 h (green), 4 h (cyan), and 8 h (purple).

near) the locations of activated furin (i.e. Golgi bodies). As a consequence of their large sizes and their hydrophobicity, which enables them to tightly attach to the membrane organelles (e.g. Golgi bodies), as-formed Taxol-NPs are difficult to pump out by Pgp and, therefore, their circulation time inside cells is prolonged effectively. After the ester bonds on Taxol-NPs are cleaved by esterases in cells, free taxol is gradually released to bind the tubulin continuously, which effectively overcomes the MDR of the cancer cells.

This strategy for overcoming the MDR of cancer cells has several merits: 1) The cell-penetrating peptide RVRR used here not only increases the water solubility of taxol, but also improves its cellular uptake and bioavailability; 2) intracellular self-assembly of Taxol-NPs not only increases the concentration of taxol locally but also prolongs its circulation time; 3) all the biocompatible materials for synthesizing CBT-Taxol and the biocompatible condensation reaction for intracellular self-assembly of taxol-NPs assure the biocompatibility of the whole strategy.

After synthesizing and characterizing CBT-Taxol (see Scheme S1 and Figure S1 in the Supporting Information), we then compared the water solubility of CBT-Taxol with taxol. As shown in Figure 2a, whereas 0.1 mM taxol was insoluble in water containing 1% DMSO, CBT-Taxol at the same concentration (i.e. 0.1 mM) was completely dissolved. When the concentration was increased to 1 mM, CBT-Taxol still dissolved in water containing 10% DMSO, while taxol at this concentration resulted in a turbid suspension. The corresponding transmittance values of vials containing 0.1 mM taxol, 0.1 mM CBT-Taxol, 1 mM taxol, and 1 mM CBT-Taxol (Figure 2a) at 600 nm were 70.0%, 99.4%, 2.30%, and 92.6%, respectively. This suggests CBT-Taxol is much soluble in water than taxol. We then validated the furin-controlled condensation of CBT-Taxol and the subsequent self-assembly of its taxol nanoparticles (Taxol-NPs). Before that, the enzymatic parameters $K_{cat}$ and $K_{cat}/K_M$ of furin towards CBT-Taxol were calculated to be 7.11 $min^{-1}$ and 0.067 $\mu M^{-1} min^{-1}$, respectively (Figure S2). After the addition of 1 mM GSH to 100 μM CBT-Taxol (dissolved in furin buffer, pH 7.0) and incubation for 2 h at 37 °C, the disulfide bond of CBT-Taxol was reduced by GSH, thereby yielding the reduction product CBT-Taxol-Red (Figure 2c and Figure S3). When 100 μM CBT-Taxol was treated with 1 mM GSH and 0.2 nmol $U^{-1}$ furin at 37 °C, the reduction product of CBT-Taxol (i.e. CBT-Taxol-Red) was gradually cleaved by furin to yield the active intermediate, which instantly condenses with each other to yield the hydrophobic dimer CBT-Taxol-Dimer (Figure 2c and Figure S4), which self-assembled into Taxol-NPs. UV/Vis spectroscopy, dynamic light scattering (DLS), and transmission electron microscope (TEM) were used to verify the formation and characterize the Taxol-NPs obtained. The increased UV/Vis absorptions from 500 nm to 700 nm (as a result of light scattering) of CBT-Taxol after incubation with furin revealed the formation of nanoparticles (Figure S5). DLS measurements showed the average hydrous dynamic diameter of as-formed Taxol-NPs was about $66.2 \pm 6.7$ nm (Figure S6). The TEM image in Figure 2b indicates that the Taxol-NPs have an average diameter of $29.8 \pm 4.3$ nm (Figure S7). To chemically validate the GSH-controlled reduction and subsequent furin-controlled condensation of CBT-Taxol, we directly subjected the above incubation mixtures to HPLC and collected the compounds for matrix-assisted laser desorption/ionization (MALDI) mass spectrometric analysis (Figure 2c). As the incubation time increased from 2 h, to 4 h, to 8 h, the ratio of the HPLC peak area of CBT-Taxol-Dimer (24.9 min, Figure S4) to CBT-Taxol-Red (21.8 min, Figure S3) increased from 0.4:1, to 1.5:1, to 60:1, thus suggesting furin cleavage is much slower than the reduction of CBT-Taxol with GSH under these conditions.

  

To validate the efficacy of CBT-Taxol for overcoming MDR, we first tested it on taxol-resistant cells. Furin-overexpressed human colon cancer HCT 116 cells (proven by Western blotting; Figure S8) were chosen for the following experiments. The 3-(4,5-dimethylthiazol-2-yl)-2,5-diphenyltetrazolium bromide (MTT) assay was employed to investigate the cytotoxicity of taxol and CBT-Taxol on parental HCT 116 cells and taxol-resistant HCT 116 cells over 48 h, respectively. However, before approaching the furin at Golgi bodies, the cyano group of CBT-Taxol would condense at a low chemical concentration with intracellular Cys, thus making its self-condensation and the assembly of Taxol-NPs unfeasible. To resolve this, we have demonstrated that co-incubation of the compound (e.g. CBT-Taxol herein) with its CBT precursor (e.g. compound **C** (Ac-Arg-Val-Arg-Arg-Cys(StBu)-Lys-2-cyanobenzothiazole) herein, see Scheme S1) above 25 μM would overcome the intracellular Cys and warrant the self-assembly of the nanoparticles inside cells.[27] We thus used 50 μM **C** for co-incubation with CBT-Taxol. To verify the intracellular self-assembly of Taxol-NPs in HCT 116 cells, we used a fluorophore Alexa 488 to replace the taxol motif on CBT-Taxol and synthesized the analogue Ac-Arg-Val-Arg-Arg-Cys(S*t*Bu)-Lys(Alexa 488)-2-cyanobenzothiazole (CBT-Alexa 488, Scheme S2 and Figure S9). After co-incubation of 5 μM CBT-Alexa 488 and 50 μM compound **C** with furin-overexpressed HCT 116 cells or furin-deficient human hepatocarcinoma SK-HEP-1 cells for 8 h, three-dimensional structured illumination microscopy (3D-SIM) fluorescence images clearly showed green fluorescent nanoparticles clustered at/near the Golgi bodies in HCT 116 cells, but very weak, homogeneously dispersed green fluorescence was displayed in SK-HEP-1 cells (Figure S10 and Movies S1–3). Cell-uptake studies indicated that, during 120 min co-incubation with 50 μM **C**, CBT-Taxol showed clearly higher cell uptakes than taxol on both HCT 116 cells and human normal liver epithelial THLE-3 cells (Figure S11). The amount of CBT-Taxol taken up by HCT 116 cancer cells was nearly twofold that of CBT-Taxol by THLE-3 normal cells (Figure S11a). The MTT assay indicated that **C** is nontoxic up to a concentration of 500 μM to both parental and taxol-resistant HCT 116 cell lines for three days (Figure S12). From Figure 3a, we find that the half-inhibitory concentration ($IC_{50}$) of taxol was 5.02 nM, and the $IC_{50}$ value of CBT-Taxol was 51.3 nM for parental HCT 116 cells. From Figure 3b, we find that the $IC_{50}$ value of taxol is 663 nM, and that of CBT-Taxol 1.51 μM for taxol-resistant HCT 116 cells. Thus, the MDR factor of CBT-Taxol was 29.4 (1.51 μM/51.3 nM), which was observably lower than the MDR factor of taxol (132 = 663 nM/5.02 nM), thus suggesting a clear anti-MDR ability of CBT-Taxol (4.5-fold of taxol). To verify that the cytotoxicity of CBT-Taxol-treated taxol-resistant HCT 116 cells resulted from furin-controlled formation of Taxol-NPs, we pretreated the cells with furin inhibitor II (H-(D)Arg-Arg-Arg-Arg-Arg-Arg-$NH_2$, 100 μM) for 30 min before incubating the cells with CBT-Taxol or taxol. The $IC_{50}$ value of CBT-Taxol-treated cells was clearly increased to 2.98 μM from its original 1.51 μM, while that of Taxol-treated cells did not change much (625 nM versus the original 663 nM; Figure S13a). This suggests that the anti-MDR effect of CBT-Taxol actually resulted from

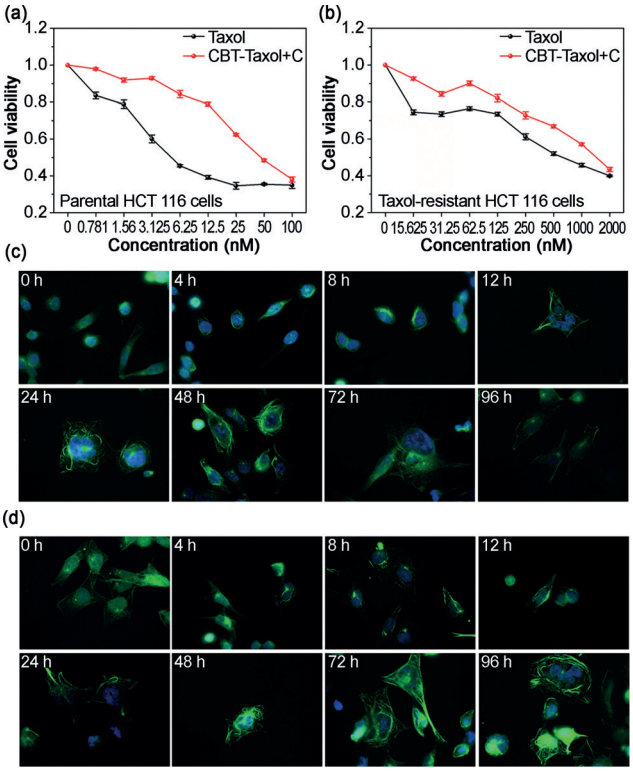


***Figure 3.*** Cell viability study of a) parental HCT 116 cells and b) taxol-resistant HCT 116 cells on treatment with taxol or CBT-Taxol (co-incubated with 50 μM **C**) for 48 h. The error bar represents the standard deviation of three independent experiments. Tubulin immunofluorescence staining of taxol-resistant HCT 116 cells treated with c) 200 nM taxol or d) 200 nM CBT-Taxol (co-incubated with 50 μM **C**) for 0 h, 4 h, 8 h, 12 h, 24 h, 48 h, 72 h, and 96 h.

furin-controlled self-assembly of Taxol-NPs. To exclude other factors (e.g. MDR1/Pgp) that probably contribute to the anti-MDR effect of CBT-Taxol on the taxol-resistant HCT 116 cells, we pretreated the cells with Pgp inhibitor (verapamil, 10 μM) for 30 min before incubating the cells with CBT-Taxol or taxol for MTT study. the $IC_{50}$ value of CBT-Taxol-treated cells was clearly decreased to 137 nM from its original 1.51 μM, while that of taxol-treated cells decreased to 24.5 nM from its original 663 nM (Figure S13b), thus suggesting CBT-Taxol did not influence the expression and function of MDR1/Pgp. To verify the furin-controlled condensation of CBT-Taxol in cells, we incubated the taxol-resistant HCT 116 cell lysate with 300 μM CBT-Taxol at 37 °C for 2 h, then the cell lysate was analyzed by HPLC. The peak of the CBT-Taxol-Dimer appeared on the HPLC trace, as expected (Figure S14). To validate the proposed anti-MDR mechanism of CBT-Taxol (i.e. long-term release of taxol from Taxol-NPs), we used the immunofluorescence staining of tubulin to track the anticancer effect of CBT-Taxol. From Figure 3c,d, we find the condensation of intracellular tubulin induced by 200 nM CBT-Taxol (co-incubated with 50 μM **C**) is slower than that with 200 nM taxol, but the duration of the tubulin-condensation induced by CBT-Taxol was longer than that by taxol. To further testify the anti-MDR effect was caused by the prolonged circulation time and the facility of cellular uptake

  

instead of down regulation of the MDR1 gene, we detected the expression level of MDR1 before and after the addition of CBT-Taxol. Neither the expression of MDR1 mRNA nor Pgp showed a noticeable change (Figure S15), thus suggesting that our CBT-Taxol did not affect the expression of the MDR1 gene.

Nude mice were subcutaneously injected with parental HCT 116 cells in the left thigh and taxol-resistant HCT 116 cells in the right thigh. When the tumor volume reached 50–100 $mm^3$, the nude mice were randomly divided into three groups ($n = 6$ for each group). Taxol or CBT-Taxol with **C** was dispersed in Cremophory/EtOH/saline (1:1:10) to 1.0 $mg\,mL^{-1}$ taxol or 2.4 $mg\,mL^{-1}$ CBT-Taxol with 5.5 $mg\,mL^{-1}$ **C**. The vehicle (Cremophory/EtOH/saline at 1:1:10) alone was used as a control. 5.0 $mg\,kg^{-1}$ Taxol (5.9 $\mu mol\,kg^{-1}$), 12 $mg\,kg^{-1}$ CBT-Taxol (5.9 $\mu mol\,kg^{-1}$) with 27.6 $mg\,kg^{-1}$ **C** (25 $\mu mol\,kg^{-1}$), or the vehicle at the same volume was injected into each nude mouse of the three groups by intraperitoneal (i.p.) injection (Q2D × 7 doses), respectively. As shown in Figure 4a, b, mice co-injected with CBT-Taxol and **C** showed impressively better antitumor effects than those only injected with taxol on both HCT 116 tumors and taxol-resistant HCT 116 tumors. At day 20, the average tumor volumes of parental HCT 116 tumors and taxol-resistant HCT 116 tumors in taxol-treated group reduced to about 56.4 % and 88.9 %, respectively, compared with those in the control group. The average tumor volumes of parental HCT 116 tumors and taxol-resistant HCT 116 tumors in the CBT-Taxol-treated group, respectively, reduced to about 33.2 % and 34.3 %, compared with those in the control group. We denoted the in vivo MDR factor as the reduction in the tumor volume ratio of taxol-resistant HCT 116 tumors to parental HCT 116 tumors. The in vivo MDR factor for taxol was 1.58 (88.9 %/56.4 %), while that for CBT-Taxol was 1.03 (34.3 %/33.2 %). Thus, we can safely conclude that CBT-Taxol co-injected with **C** has a clear anti-MDR effect on the taxol-resistant tumors (1.53-fold increase of the anti-MDR factor of taxol). The tumor weights obtained from the above three groups at day 20 were consistent with the above results on the tumor volume (Figure 4c; typical photographs of tumors of three groups at day 20 are shown in Figure S16). During treatment, we measured the body weight of each mouse to validate the toxicity of the drugs (or vehicle). As shown in Figure 4d, compared with that of the control group, the average body weight of taxol-treated mice at day 20 reduced by about 9.1 %, thus indicating that taxol is toxic to mice at this injection dose. Interestingly, the average body weight of mice in the group treated with CBT-Taxol and **C** at day 20 increased by about 6.1 %, compared with that of the control group, thus suggesting CBT-Taxol with **C** remitted the toxicity of the vehicle on the mice. The above results indicated that while CBT-Taxol co-injected with **C** showed better anti-MDR properties on taxol-resistant tumors than taxol, it was not toxic to the mice.

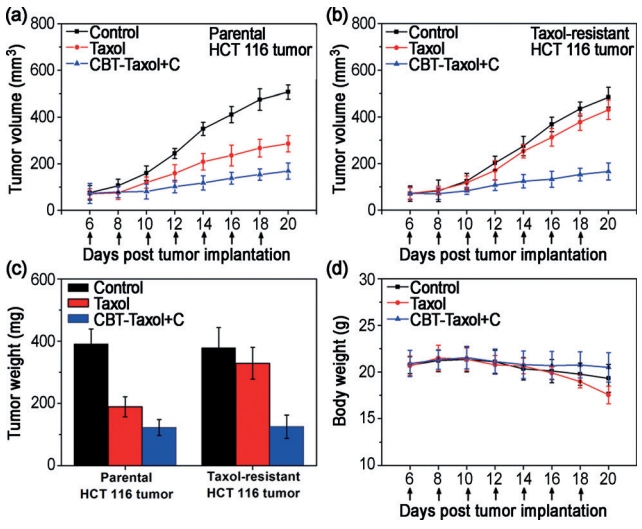


***Figure 4.*** Antitumor effect of control vehicle, taxol, and CBT-Taxol co-injected with **C** on a) parental HCT 116 tumor or b) taxol-resistant HCT 116 tumor implanted in nude mice. c) Tumor weight of nude mice implanted with parental HCT 116 tumors and taxol-resistant HCT 116 tumors at day 20 when treated with control vehicle, taxol, and CBT-Taxol co-injected with **C**. d) Change in mouse body weight versus time. The arrow indicates that each mouse receives one dose of injection at this time point.

In summary, based on a biocompatible condensation reaction and enzymatic self-assembly, we rationally designed a taxol derivative CBT-Taxol and offered a new strategy for overcoming MDR. A MTT study indicated that, compared with taxol, CBT-Taxol co-incubated with **C** has a 4.5-fold increased anti-MDR effect on taxol-resistant HCT 116 cancer cells. Immunofluorescence microscopic cell imaging indicated that CBT-Taxol has a longer lasting effect on tubulin condensation than taxol, thus suggesting intracellular self-assembly of Taxol-NPs and slow release of taxol from the nanoparticles. In vivo studies indicated that co-injection of CBT-Taxol with **C** showed a 1.53-fold increase in the anti-MDR effect on taxol-resistant HCT 116 tumors than taxol, while not being toxic to the mice. With these in vitro and in vivo anti-MDR effects of CBT-Taxol, we envision our strategy to be a starting point for scientists to design more sophisticated intracellular self-assembling systems for treating diseases and overcoming MDR more efficiently.

**Keywords:** furin · multidrug resistance · nanoparticles · self-assembly · taxol

**How to cite:** *Angew. Chem. Int. Ed.* **2015**, *54*, 9700–9704
*Angew. Chem.* **2015**, *127*, 9836–9840

[1] E. K. Pauwels, P. Erba, G. Mariani, C. M. Gomes, *Drug News Perspect.* **2007**, *20*, 371–377.
[2] M. M. Gottesman, T. Fojo, S. E. Bates, *Nat. Rev. Cancer* **2002**, *2*, 48–58.
[3] M. Filipits, *Drug Discovery Today Dis. Mech.* **2004**, *1*, 229–234.
[4] F. J. Sharom, X. Yu, P. Lu, R. Liu, J. W. Chu, K. Szabo, M. Muller, C. D. Hose, A. Monks, A. Varadi, J. Seprodi, B. Sarkadi, *Biochem. Pharmacol.* **1999**, *58*, 571–586.
[5] E. B. Mechetner, I. B. Roninson, *Proc. Natl. Acad. Sci. USA* **1992**, *89*, 5824–5828.
[6] Z. Wang, Z. Wang, D. Liu, X. Yan, F. Wang, G. Niu, M. Yang, X. Chen, *Angew. Chem. Int. Ed.* **2014**, *53*, 1997–2001; *Angew. Chem.* **2014**, *126*, 2028–2032.
[7] D. Xu, D. Ye, M. Fisher, R. L. Juliano, *J. Pharmacol. Exp. Ther.* **2002**, *302*, 963–971.

[8] M. Susa, A. K. Iyer, K. Ryu, E. Choy, F. J. Hornicek, H. Mankin, L. Milane, M. M. Amiji, Z. Duan, *PLoS One* **2010**, *5*, e10764.
[9] J. Perez, C. Bardin, C. Rigal, B. Anthony, R. Rousseau, A. Dutour, *Anticancer Res.* **2011**, *31*, 2813 – 2820.
[10] G. L. Semenza, *Cancer Cell* **2004**, *5*, 405 – 406.
[11] D. M. Bollag, P. A. McQueney, J. Zhu, O. Hensens, L. Koupal, J. Liesch, M. Goetz, E. Lazarides, C. M. Woods, *Cancer Res.* **1995**, *55*, 2325 – 2333.
[12] S. L. Mooberry, G. Tien, A. H. Hernandez, A. Plubrukarn, B. S. Davidson, *Cancer Res.* **1999**, *59*, 653 – 660.
[13] Y. Min, J. Li, F. Liu, E. K. L. Yeow, B. Xing, *Angew. Chem. Int. Ed.* **2014**, *53*, 1012 – 1016; *Angew. Chem.* **2014**, *126*, 1030 – 1034.
[14] J. L. Markman, A. Rekechenetskiy, E. Holler, J. Y. Ljubimova, *Adv. Drug Delivery Rev.* **2013**, *65*, 1866 – 1879.
[15] E. A. Dubikovskaya, S. H. Thorne, T. H. Pillow, C. H. Contag, P. A. Wender, *Proc. Natl. Acad. Sci. USA* **2008**, *105*, 12128 – 12133.
[16] L. van Zuylen, K. Nooter, A. Sparreboom, J. Verweij, *Invest. New Drugs* **2000**, *18*, 205 – 220.
[17] I. Ojima, J. C. Slater, E. Michaud, S. D. Kuduk, P. Y. Bounaud, P. Vrignaud, M. C. Bissery, J. M. Veith, P. Pera, R. J. Bernacki, *J. Med. Chem.* **1996**, *39*, 3889 – 3896.
[18] L. D. Mayer, *Cancer Metastasis Rev.* **1998**, *17*, 211 – 218.
[19] E. A. Goun, T. H. Pillow, L. R. Jones, J. B. Rothbard, P. A. Wender, *ChemBioChem* **2006**, *7*, 1497 – 1515.
[20] R. H. H. Neubert, *Eur. J. Pharm. Biopharm.* **2011**, *77*, 1 – 2.
[21] G. Liang, H. Ren, J. Rao, *Nat. Chem.* **2010**, *2*, 54 – 60.
[22] G. Liang, J. Ronald, Y. Chen, D. Ye, P. Pandit, M. L. Ma, B. Rutt, J. Rao, *Angew. Chem. Int. Ed.* **2011**, *50*, 6283 – 6286; *Angew. Chem.* **2011**, *123*, 6407 – 6410.
[23] Y. Yuan, H. Sun, S. Ge, M. Wang, H. Zhao, L. Wang, L. An, J. Zhang, H. Zhang, B. Hu, J. Wang, G. Liang, *ACS Nano* **2015**, *9*, 761 – 768.
[24] C. Cao, Y. Shen, J. Wang, L. Li, G. Liang, *Sci. Rep.* **2013**, *3*, 1024.
[25] A. El-Sayed, S. Futaki, H. Harashima, *AAPS J.* **2009**, *11*, 13 – 22.
[26] G. Thomas, *Nat. Rev. Mol. Cell Biol.* **2002**, *3*, 753 – 766.
[27] Q. Miao, X. Bai, Y. Shen, B. Mei, J. Gao, L. Li, G. Liang, *Chem. Commun.* **2012**, *48*, 9738 – 9740.

Received: May 12, 2015
Published online: June 26, 2015

  